Research Article | Vol. 10, No. 2 / 1 February 2020 / Optical Materials Express 302
Optical Materials EXPRESS

Enlarged growth window for plasmonic silicon-doped InAs using a bismuth surfactant

Dongxia Wei,[1] Scott Maddox,[2] Patrick Sohr,[1] Seth Bank,[2,3] and Stephanie Law[1,4]

[1]Department of Materials Science and Engineering, University of Delaware, 127 The Green Room 201, Newark DE 19716, USA
[2]Department of Electrical and Computer Engineering, University of Texas at Austin, 10100 Burnet Road, Building 160, Austin, TX 78758, USA
[3]sbank@utexas.edu
[4]slaw@udel.edu

Abstract: Semiconductors such as InAs with high dopant concentrations have a variety of applications, including as components of mid-infrared optoelectronic devices. Unfortunately, growth of these materials by molecular beam epitaxy is challenging, requiring high growth rates and low growth temperatures. We show that the use of a bismuth surfactant improves silicon incorporation into InAs while simultaneously reducing the optical scattering rate, increasing the carrier mobility, reducing surface roughness, and enabling growth at higher substrate temperatures and slower growth rates. We explain our findings using microscopic theories of dopant segregation and defect formation in III-V materials.

1. Introduction

The mid-infrared (MIR) is a technologically important wavelength range for a variety of applications in sensing, imaging, and defense [1]. This is because the MIR contains the unique vibrational and rotational absorption spectra for a variety of molecules of interest in addition to thermal radiation across a wide range of temperatures. A large number of semiconductor-based optical devices have become available in this wavelength range in the past decade, including quantum cascade lasers, type-II superlattice detectors, and a variety of passive optical components. Unfortunately, the large free-space wavelength of MIR radiation generally requires relatively large optical devices. One way to decrease the size of these devices as well as create on-chip MIR systems is by leveraging plasmonic structures. Plasmonic and metamaterial structures in the visible spectral range have shown great promise when integrated with the existing visible optical infrastructure. However, traditional visible plasmonic materials like gold and silver are not as effective in the MIR, due to their large, negative permittivities. Instead, we must use alternative materials.

Doped III-V semiconductors have been shown to be good designer plasmonic metals in the MIR, enabling light confinement at the subwavelength scale [2–8]. These materials have been used to create layered hyperbolic metamaterials, enhanced infrared detectors, subwavelength antennas, and environmental sensors [4,9–13]. One of the major advantages of using doped semiconductors as MIR plasmonic materials is the ability to natively integrate plasmonic structures with active devices during a single growth, enabling easy fabrication and minimizing losses [14,15]. Among the III-V semiconductors, silicon-doped InAs is widely used, due to its extremely high maximum doping level and small electron effective mass, leading to some of the shortest plasma wavelengths in this material class. Unfortunately, the growth of highly-doped InAs with good optical quality by molecular beam epitaxy is not easy because the silicon donor atoms tend to surface-segregate at high doping densities, leading to defects in the structure [16–18]. Significant surface roughening occurs, leading to large optical scattering rates and low electron mobilities. A fast growth

#383260 https://doi.org/10.1364/OME.383260
Journal © 2020 Received 15 Nov 2019; revised 19 Dec 2019; accepted 19 Dec 2019; published 3 Jan 2020

Optical Materials EXPRESS

rate (>1.5μm/hour) and a relatively low growth temperature (below ~450°C), are needed to incorporate silicon dopants above a density of $\sim 1 \times 10^{19}$ cm^{-3} while maintaining good material quality. Because the growth window is extremely narrow, it is difficult to reproducibly grow Si:InAs with doping densities higher than $\sim 1 \times 10^{19}$ cm^{-3}. In addition, other lattice-matched III-V semiconductors, like AlSb and GaSb, favor a higher growth temperature (over 500°C). The strict growth conditions of highly-doped InAs make growth challenging and limit its ability to be integrated with other III-V semiconductor devices. To date, the microscopic mechanism behind the surface roughening observed in heavily-doped InAs has not been explored.

One common way to improve material growth generally is by using surfactants. The use of bismuth as a surfactant has been reported for the epitaxial growth of germanium [19], InAs quantum dots [20–22], GaAs-InGaAs heterostructures [23], InAsSb [24,25], and many more systems [26–28]. Bismuth improves the growth of III-V semiconductors by suppressing the diffusion of group III atoms, preventing the 3D growth mode [29–31]. A key advantage of bismuth as a surfactant is that it does not incorporate into III-V semiconductors unless the growth temperature is below 350°C [32,33]. Other surfactants like tellurium [34,35] and antimony [36,37] will either introduce significant defect levels or incorporate into the lattice.

In this paper, we investigate the surfactant effect of bismuth on the growth of silicon-doped InAs. We show that the use of small amounts of bismuth reduces surface roughness, lowers the optical scattering rate by a factor of two, and improves silicon incorporation. In addition, we find that using a bismuth surfactant enables high-quality growth of Si:InAs at higher substrate temperatures and at slower growth rates, paving the way for incorporation of this plasmonic material with existing optical devices in the 6.1 Å family. The relaxed growth conditions also enable more reproducible material growth. We explain our results using a microscopic model of dopant incorporation that includes Coulomb repulsion between the ions, Fermi level pinning effects, and defect formation.

2. Methods

All samples were grown by molecular beam epitaxy (MBE) directly on semi-insulating GaAs substrates. GaAs and InAs have about a 7% lattice mismatch. While this large lattice mismatch is not ideal, it is still possible to grow high quality InAs on GaAs. It has been shown that when growing GaSb, which has a similar lattice constant to InAs, on GaAs, the GaSb relaxes to form primarily 90° dislocations at the interface under the right growth conditions [38]. Additionally, it has been shown any defects from the lattice mismatch have little effect on the carrier concentration of the Si:InAs [2]. The first set of samples (shown in Fig. 1) were grown at a constant substrate temperature of 380°C and an As_2:In beam equivalent pressure (BEP) ratio of 13. This first set of samples had a thickness of approximately 500 nm. Some samples were grown with an additional constant bismuth flux of 5×10^{-7} Torr giving Bi:In flux ratios of 0-4% depending on growth rate. A second set of samples (Figs. 2, 3, and 4) were grown with an As_2:In BEP ratio of 6.5, Bi:In flux ratios varing from 0% to 4%, and growth temperatures ranging from 450°C to 550°C. These sets of samples were all around 1μm thick. The InAs growth rate and silicon cell temperature were constant for this second set of samples. We use a Bruker Vertex 70 V Fourier transform infrared spectroscopy (FTIR) to collect reflection spectra at a nearly-normal, 10 degree incident angle using a DTGS detector with a spectral resolution of 4cm^{-1} and a scan velocity of 10kHz. The reflection data is normalized to reflection from a gold mirror set at the same angle. The plasma frequency, ω_p, and the scattering rate, Γ, are extracted from the reflection data using a transfer matrix method in which the Si:InAs is modeled as a Drude material:

$$\varepsilon_{Si:InAs} = \varepsilon_s \left(1 - \frac{\omega_p^2}{\omega^2 + i\omega\Gamma}\right) \tag{1}$$

Optical Materials EXPRESS

where ε_s is the high-frequency permittivity of the undoped InAs and ω is the frequency of incident light. Room temperature Hall effect measurements are performed using a custom-built four-point van der Pauw setup to obtain the bulk carrier density (n_{3D}) and the mobility (μ).

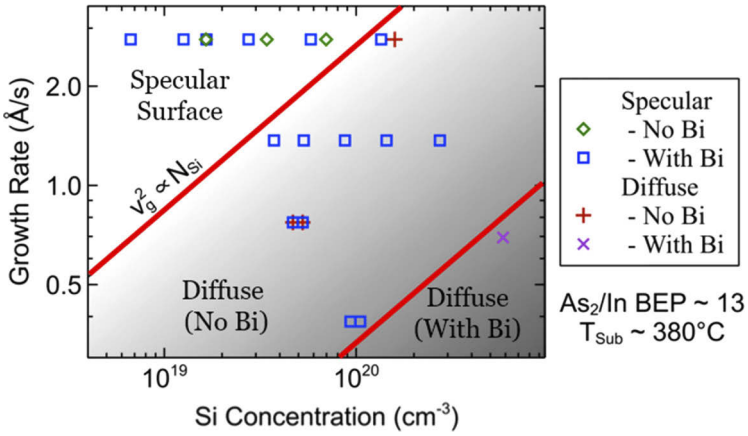

Fig. 1. Film surface quality as a function of growth rate and silicon concentration for films grown with a bismuth surfactant (blue squares and purple crosses) and without (green diamonds and red plusses). Films either show a specular surface (green diamonds and blue squares) or a diffuse surface (red plusses and purple crosses).

3. Results and discussion

As previously discussed, high growth rates have been used to incorporate large densities of silicon dopants into InAs while retaining a smooth surface. However, large fluxes can be difficult to maintain, and high growth rates are not always practical. In Fig. 1, we show data for Si:InAs films in which the growth rate and silicon flux were varied while the substrate temperature was held constant. Some samples were grown with a bismuth flux of 5×10^{-7} Torr, while others were grown without bismuth. For samples with a relatively high growth rate (>2.0 Å/s) and silicon concentrations below 1×10^{20} cm^{-3}, the films were smooth with or without the bismuth flux (blue squares and green diamonds, respectively). However, for samples grown without bismuth at lower growth rates or with larger silicon fluxes, the surfaces were rough (red plusses). Under identical growth conditions using the bismuth surfactant, the surface became smooth and specular again. With the bismuth surfactant, specular surfaces with silicon concentrations of greater than 10^{20} cm^{-3} were achieved, a record for this material system. At extremely high silicon concentrations, the surface is rough even with the bismuth surfactant (purple cross). However, the use of bismuth substantially increases the growth window for high optical quality films at low substrate temperatures. For all samples, the silicon concentration was determined with Hall effect measurements. Additionally, we verified that there was no bismuth present in the Si:InAs films after growth using electron diffraction spectroscopy (EDS), which has a detection limit around 0.5wt%.

In the second set of samples, the growth rate and silicon flux are held constant while the substrate temperature and bismuth flux are varied. The electrical and optical properties for these samples are plotted in Fig. 2. In Fig. 2(a) and (b), we plot the carrier density and mobility, respectively, for samples grown with varying bismuth fluxes at substrate temperatures ranging from 450°C to 550°C. Filled symbols indicate samples with a specular reflective surface, while open symbols indicate a diffuse cloudy surface. The dotted line in Fig. 2(a) indicates the nominal flux of silicon atoms. This flux was determined by growing InAs calibration wafers using the

Optical Materials EXPRESS

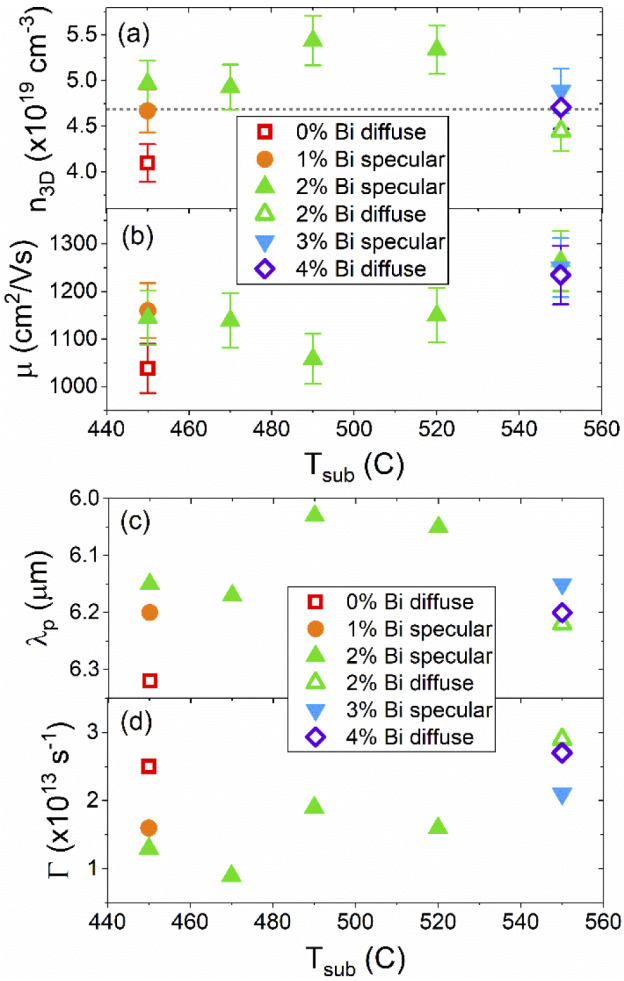

Fig. 2. Carrier density (a) and mobility (b) as determined by Hall measurements and plasma wavelength (c) and scattering rate (d) as determined by optical measurements as a function of substrate temperature for samples grown with no bismuth (red square), 1% bismuth (orange circle), 2% bismuth (green up triangle), 3% bismuth (blue down triangle), and 4% bismuth (purple diamond). Filled symbols indicate samples with a specular surface; open symbols indicate a diffuse surface. Dotted line in (a) indicates the nominal flux of silicon atoms.

same silicon effusion cell conditions and performing Hall measurements to extract the carrier density. We assumed a silicon incorporation and ion ionization efficiency in our calibration films of 100%. The film grown without the use of bismuth at 450°C (red square) shows a diffuse surface, with a low carrier density and a low mobility. However, adding a flux of 1% bismuth (orange circle) increases the carrier density to the expected value, increases the mobility, and leads to a specular surface. An increase in bismuth flux to 2% (green upward triangle) further increases the carrier density, with no effect on the sample mobility to within error bars. This is likely caused by improved substitution of silicon atoms on the group III site compared to the silicon dopant incorporation in our calibration film. Bismuth is known to improve incorporation and reduce surface segregation in other material systems [23,39–41]. It is therefore reasonable to assume that the bismuth surfactant has helped improve silicon incorporation in this case as well, thereby leading to a slightly higher than expected doping density. The use of the 2%

Optical Materials EXPRESS

bismuth flux also allows us to increase our growth temperature while maintaining a specular surface. At intermediate growth temperatures, we observe a small increase in carrier density with a corresponding decrease in mobility, possibly due to an increase in scattering from incorporated ionized impurities. Finally, when we reach a substrate temperature of 550°C, samples grown with 2% bismuth show a diffuse surface, with a decrease in carrier density. By increasing the bismuth flux to 3%, we recover a specular surface and increase the carrier density slightly. However, increasing the bismuth flux further to 4% results in a diffuse surface. Interestingly, all three samples grown at 550C show the highest mobilities, with no difference (to within error bars) among the samples. We attribute this to improved crystallinity of the InAs film when grown at these high temperatures.

In Fig. 2(c) and (d), we show the plasma wavelength and scattering rate, respectively. The trends in these data are similar to those shown in Fig. 2(a) and (b), with shorter plasma wavelengths obtained at higher substrate temperatures with a bismuth flux. Since the plasma wavelength is proportional to the free carrier density, this is as expected. However, the scattering rate does not precisely mirror the mobility. Although this may appear surprising at first glance, it can be explained by noting that the mobility is a DC measurement, while the scattering rate is measured at high optical frequencies. Therefore, it is not unreasonable for these two measurements to differ slightly.

The use of a bismuth surfactant improves both the electrical and optical properties of silicon-doped InAs films. To understand this effect, we must first discuss the microscopic behavior of silicon dopants in III-V systems. To date, most investigations have been in the silicon-doped GaAs system; we will use much of this formalism in our discussion of silicon-doped InAs. We will also focus solely on n-type silicon doping. The upper doping limit depends on the growth temperature, the III:V ratio, and the growth rate as well as the material-specific intrinsic Fermi level stabilization point. One major driving force controlling the maximum electron concentration in III-V materials is the Coulomb repulsion between the ionized donor cores [42]. The surface Fermi level for most III-V semiconductors is pinned, leading to a surface accumulation or depletion region. This sets up an electric field near the surface of the film. The silicon atoms within the III-V material are ionized, leading to a Coulomb repulsion between the atoms. The combination of the Coulomb repulsion and the surface electric field drives charged impurities to drift toward the surface, where they accumulate. Using this model, the maximum impurity concentration will be obtained with the growth rate equals the impurity drift velocity toward the surface. Higher growth rates should therefore result in larger maximum dopant densities, as we observe in Fig. 1. In addition, this theory predicts a quadratic relationship between growth rate and dopant incorporation. The red line drawn in Fig. 1 separating smooth and rough films grown without bismuth shows this quadratic dependence, indicating that Coulomb repulsion between ionized donor cores is a significant factor contributing to surface roughening. The use of a bismuth surfactant generally suppresses the surface adatom mobility, reducing the surface free energy thereby reducing the diffusion of silicon atoms toward the surface. Bismuth surfactants can therefore improve the incorporation of silicon atoms into the III-V matrix, shifting this red line to the left, as shown in Fig. 1.

In addition to surface roughening caused by Coulomb repulsion, we must also consider defect formation. The behavior of silicon in GaAs is extremely complex: multiple defect states are possible, including Si_{Ga}, Si_{As}, Si_{Ga}-Si_{As} pairs, Si_{Ga}-V_{Ga} pairs, and other less-common higher-order defect and vacancy complexes [43]. Multiple authors have found that the doping of semiconductors follows a “pinning” rule. When a material is doped, its Fermi level rises into the conduction band until it reaches the pinning energy, after which it is impossible to raise the Fermi level further [44,45]. This is due to the formation of defects that compensate the intentional dopants. By raising the Fermi energy into the conduction band, the formation enthalpy of intrinsic acceptor defects is reduced. These compensating defects have been identified as

Optical Materials EXPRESS

closed shell acceptor defects, for which the energy required to form the defect states is canceled by the energy required to occupy them [45]. This will limit the doping for InAs specifically to $\sim 1 \times 10^{20}$ cm^{-3}, regardless of growth rate. However, this limitation can be overcome by kinetically inhibiting the formation of such defects by growing at low substrate temperatures; this technique has successfully been used for Si:InAs. However, as shown in Fig. 2, the change in growth kinetics with the addition of bismuth will suppress the formation of compensating defects, enabling growth at higher substrate temperatures. Specifically, calculations show that the major compensating defects in most III-V materials are cation vacancies and DX centers. Bismuth acts to help incorporate group III elements, which will lead to a concomitant reduction in cation vacancies, suppressing the formation of these defect complexes. In this way, bismuth allows us to move the Fermi energy above the pinning energy while also promoting silicon atom incorporation into the lattice, resulting in an increase in carrier density even at high substrate temperatures.

In addition to measuring the optical and electrical properties of the samples shown in Fig. 2, we also investigated their surface morphology using optical microscopy, scanning electron microscope (SEM), and atomic force microscopy (AFM). These data are shown in Fig. 3. For the sample grown without bismuth (Fig. 3(a)), we observe many dark spots under the optical microscope, corresponding to the diffuse surface. SEM (inset, Fig. 3(a)) and AFM (Fig. 4(a)) images collected on this sample show that the dark spots are actually deep trenches elongated along the [110] direction. We hypothesize that these trenches are actually large clusters of silicon atoms. In heavily silicon-doped GaAs, similar trenches have been observed in both transmission electron microscopy and scanning tunneling microscopy measurements [46,47]. The observed trenches were elongated along the [110] direction and their length corresponded to the density of silicon atoms as well as the growth temperature; higher densities led to more and longer trenches. The observed trenches in our heavily-doped InAs show characteristics similar to those observed in GaAs, including elongation along the same crystal axes. It is therefore reasonable to assume

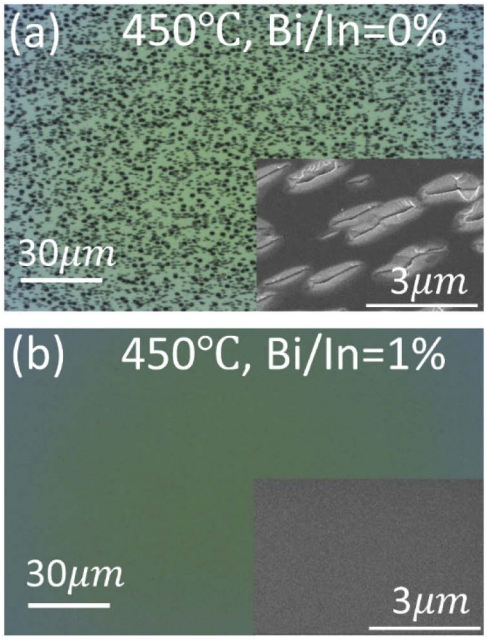

Fig. 3. Optical microscope images for samples grown at 450C with bismuth fluxes of 0% (a) and 1% (b). Insets show corresponding scanning electron microscope images. Rectangular trenches are observed in (a), while (b) is featureless.

Optical Materials EXPRESS

that they are also caused by a similar mechanism, namely silicon aggregating on the surface. In Fig. 3(b), we show images collected from the sample grown at 450°C with a Bi/In flux ratio of 1%. This sample appeared shiny to the eye and was smooth and featureless under both optical microscopy and SEM, with no observable trenches. We can attribute this to the change in surface energy due to the presence of the surfactant leading to a reduction in silicon diffusion toward the surface. Since the silicon atoms are incorporating into the lattice rather than accumulating at the surface, the trenches due to silicon clustering have disappeared.

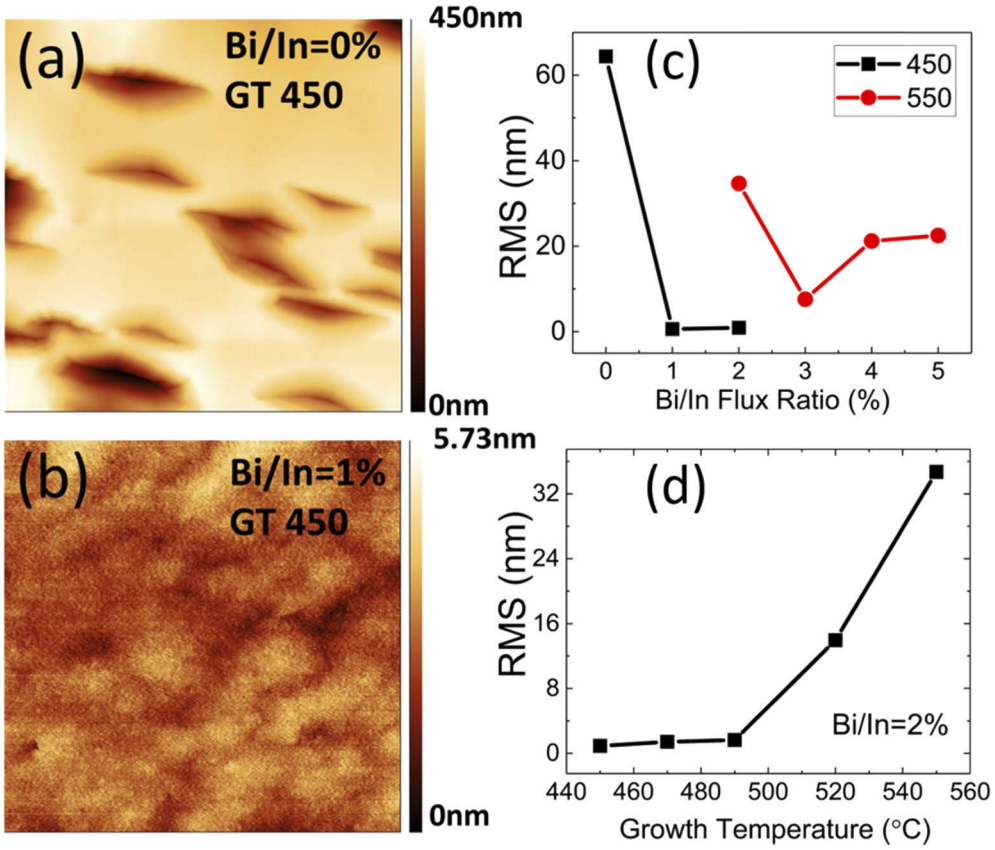

Fig. 4. Atomic force microscope images for samples grown at 450C with bismuth fluxes of 0% (a) and 1% (b). Note the difference in scale. (c) RMS roughness as a function of growth temperature for samples grown with a bismuth flux of 2%; surface roughness increases above ~500C. (d) RMS roughness as a function of bismuth flux for samples grown at 450C (black squares) and 550C (red circles).

Finally, we collected AFM images and calculated the root mean square (RMS) roughness for all samples shown in Fig. 2; these data are presented in Fig. 4. Figure 4(a) and 4(b) show AFM scans for samples grown at a substrate temperature of 450°C and Bi/In flux ratios of 0% and 1%, respectively. The sample grown with the bismuth surfactant is smooth and featureless, while the sample without bismuth exhibits elongated deep trenches, consistent with the images presented in Fig. 3(a) and (b). Figure 4(c) plots the RMS roughness for samples grown at either 450°C (black squares) or 550°C (red circles) as a function of bismuth flux. The RMS roughness of samples grown at 450°C drops from 64.4nm to less than 0.7nm when the Bi/In flux ratio changes from 0% to 1%, indicating a significant smoothing effect caused by the bismuth surfactant. For samples grown at 550°C, the RMS roughness is lowest for a 3% bismuth flux. This sample is the only one

Optical Materials EXPRESS

grown at 550°C that is shiny to the eye; it also shows the lowest scattering rate of this group of samples. At higher bismuth fluxes, the RMS roughness increases again. Finally, in Fig. 4(d), we show the RMS roughness as a function of growth temperature for samples grown with a bismuth flux of 2%. The RMS roughness remains below 15nm when the growth temperature is below 520°C, but at higher temperatures, the RMS roughness increases significantly.

Taken together, these data suggest multiple mechanisms for surface roughening. At low temperatures and low bismuth ratios, elongated trenches form due to silicon clustering at the surface, as previously described. At moderate bismuth fluxes (Fig. 4(c) black squares), RMS roughness decreases due to the surfactant effect whereby bismuth not only suppress the mobility of group III atoms, it also suppresses the redistribution of silicon atoms which tend to surface-segregate. At constant bismuth flux (Fig. 4(d)), the surface roughness increases as the temperature increases due to thermal roughening and an increase in arsenic desorption. Finally, when large bismuth fluxes are used at a constant temperature (Fig. 4(c) red circles), bismuth-indium complexes can form during the growth, resulting in a rougher surface [27]. This interplay between bismuth flux and substrate temperature sets up a competition among these effects, resulting in a variety of parameters combining to give similar effects.

4. Conclusions

In conclusion, we have studied the effect of a bismuth surfactant on the electrical, optical, and structural properties of heavily silicon-doped InAs films grown using molecular beam epitaxy. A small bismuth flux can lower the scattering rate, increase silicon incorporation, and improve the surface morphology of highly doped InAs films. The reduced scattering is crucial for the development of low-loss plasmonic structures in the mid-infrared. In addition, the use of bismuth as a surfactant enlarges the growth window, allowing the growth of high-quality material at much lower growth rates and at much higher substrate temperatures. This is crucial for reproducibly obtaining high-quality plasmonic InAs and for the epitaxial integration of highly-doped InAs with other lattice-matched semiconductors (GaSb, AlSb) and optoelectronic devices.

Funding

Directorate for Mathematical and Physical Sciences (1606673); Air Force Office of Scientific Research (FA9550-12- 1-0488).

Acknowledgments

We would also like to thank J. Zhang and J. Zide at the University of Delaware for helpful conversations.

Disclosures

The authors declare no conflicts of interest.

References

1. S. Law, V. Podolskiy, and D. Wasserman, "Towards nano-scale photonics with micro-scale photons: the opportunities and challenges of mid-infrared plasmonics," Nanophotonics **2**(2), 103–130 (2013).
2. S. Law, R. Liu, and D. Wasserman, "Doped semiconductors with band-edge plasma frequencies," J. Vac. Sci. Technol., B: Nanotechnol. Microelectron.: Mater., Process., Meas., Phenom. **32**(5), 052601 (2014).
3. S. Law, L. Yu, and D. Wasserman, "Epitaxial growth of engineered metals for mid-infrared plasmonics," J. Vac. Sci. Technol., B: Nanotechnol. Microelectron.: Mater., Process., Meas., Phenom. **31**(3), 03C121 (2013).
4. S. Law, L. Yu, A. Rosenberg, and D. Wasserman, "All-semiconductor plasmonic nanoantennas for infrared sensing," Nano Lett. **13**(9), 4569–4574 (2013).
5. S. Law, D. C. Adams, A. M. Taylor, and D. Wasserman, "Mid-infrared designer metals," Opt. Express **20**(11), 12155–12165 (2012).

Optical Materials EXPRESS

6. V. N. Guilengui, L. Cerutti, J. B. Rodriguez, E. Tournie, and T. Taliercio, "Localized surface plasmon resonances in highly doped semiconductors nanostructures," Appl. Phys. Lett. **101**(16), 161113 (2012).
7. T. Taliercio, V. N. Guilengui, L. Cerutti, E. Tournié, and J.-J. Greffet, "Brewster "mode" in highly doped semiconductor layers: an all-optical technique to monitor doping concentration," Opt. Express **22**(20), 24294–303 (2014).
8. T. Taliercio, V. N. Guilengui, L. Cerutti, J.-B. Rodriguez, F. Barho, M.-J. M. Rodrigo, F. Gonzalez-Posada, E. Tournié, M. Niehle, and A. Trampert, "Fano-like resonances sustained by Si doped InAsSb plasmonic resonators integrated in GaSb matrix," Opt. Express **23**(23), 29423 (2015).
9. A. J. Hoffman, L. Alekseyev, S. S. Howard, K. J. Franz, D. Wasserman, V. A. Podolskiy, E. E. Narimanov, D. L. Sivco, and C. Gmachl, "Negative refraction in semiconductor metamaterials," Nat. Mater. **6**(12), 946–950 (2007).
10. D. Wei, C. Harris, C. C. Bomberger, J. Zhang, J. Zide, and S. Law, "Single-material semiconductor hyperbolic metamaterials," Opt. Express **24**(8), 8735–8745 (2016).
11. M. Desouky, A. M. Mahmoud, and M. A. Swillam, "Tunable Mid IR focusing in InAs based semiconductor Hyperbolic Metamaterial," Sci. Rep. **7**(1), 15312 (2017).
12. K. Feng, G. Harden, D. L. Sivco, and A. J. Hoffman, "Subdiffraction Confinement in All-Semiconductor Hyperbolic Metamaterial Resonators," ACS Photonics **4**(7), 1621–1626 (2017).
13. H. R. Seren, J. Zhang, G. R. Keiser, S. J. Maddox, X. Zhao, K. Fan, S. R. Bank, X. Zhang, and R. D. Averitt, "Nonlinear terahertz devices utilizing semiconducting plasmonic metamaterials," Light: Sci. Appl. **5**(5), e16078 (2016).
14. D. Li and C. Z. Ning, "All-semiconductor active plasmonic system in mid-infrared wavelengths," Opt. Express **19**(15), 14594 (2011).
15. M. Wagner, A. S. Mcleod, S. J. Maddox, Z. Fei, M. Liu, R. D. Averitt, M. M. Fogler, S. R. Bank, F. Keilmann, and D. N. Basov, "Ultrafast Dynamics of Surface Plasmons in InAs by Time-Resolved Infrared Nanospectroscopy," Nano Lett. **14**(8), 4529–4534 (2014).
16. Y. S. Fatt, "Evidence of silicon segregation as a function of arsenic overpressure in GaAs grown by molecular beam epitaxy," J. Appl. Phys. **72**(7), 2846–2849 (1992).
17. H. Yamaguchi and Y. Horikoshi, "Surface-defect formation on heavily doped InAs and GaAs layers studied by scanning tunneling microscopy," Phys. Rev. B **53**(8), 4565–4569 (1996).
18. E. F. Schubert, J. M. Kuo, R. F. Kopf, A. S. Jordan, H. S. Luftman, and L. C. Hopkins, "Fermi-level-pinning-induced impurity redistribution in semiconductors during epitaxial growth," Phys. Rev. B **42**(2), 1364–1368 (1990).
19. A. Kawano, I. Konomi, H. Azuma, T. Hioki, and S. Noda, "Influence of bismuth as a surfactant on the growth of germanium on silicon," J. Appl. Phys. **74**(6), 4265–4267 (1993).
20. V. D. Dasika, E. M. Krivoy, H. P. Nair, S. J. Maddox, K. W. Park, D. Jung, M. L. Lee, E. T. Yu, and S. R. Bank, "Increased InAs quantum dot size and density using bismuth as a surfactant," Appl. Phys. Lett. **105**(25), 253104 (2014).
21. D. Fan, Z. Zeng, V. G. Dorogan, Y. Hirono, C. Li, Y. I. Mazur, S.-Q. Yu, S. R. Johnson, Z. M. Wang, and G. J. Salamo, "Bismuth surfactant mediated growth of InAs quantum dots by molecular beam epitaxy," J. Mater. Sci.: Mater. Electron. **24**(5), 1635–1639 (2013).
22. B. N. Zvonkov, I. A. Karpovich, N. V. Baidus, D. O. Filatov, S. V. Morozov, and Y. Y. Gushina, "Surfactant effect of bismuth in the MOVPE growth of the InAs quantum dots on GaAs," Nanotechnology **11**(4), 221–226 (2000).
23. M. R. Pillai, S.-S. Kim, S. T. Ho, and S. A. Barnett, "Growth of In_xGa_{1-x} As/GaAs heterostructures using Bi as a surfactant," J. Vac. Sci. Technol., B: Microelectron. Process. Phenom. **18**(3), 1232 (2000).
24. E. M. Anderson, A. M. Lundquist, W. L. Sarney, S. P. Svensson, P. J. Carrington, C. Pearson, and J. M. Millunchick, "Influence of a Bi surfactant on Sb incorporation in InAsSb alloys," J. Appl. Phys. **116**(1), 014901 (2014).
25. P. T. Webster, N. A. Riordan, C. Gogineni, S. Liu, J. Lu, X.-H. Zhao, D. J. Smith, Y.-H. Zhang, and S. R. Johnson, "Molecular beam epitaxy using bismuth as a constituent in InAs and a surfactant in InAs/InAsSb superlattices," J. Vac. Sci. Technol., B: Nanotechnol. Microelectron.: Mater., Process., Meas., Phenom. **32**(2), 02C120 (2014).
26. E. C. Young, S. Tixier, and T. Tiedje, "Bismuth surfactant growth of the dilute nitride GaNxAs1−x," J. Cryst. Growth **279**(3-4), 316–320 (2005).
27. Y. Gu, Y. G. Zhang, X. Y. Chen, S. P. Xi, B. Du, and Y. J. Ma, "Effect of bismuth surfactant on InP-based highly strained InAs/InGaAs triangular quantum wells," Appl. Phys. Lett. **107**(21), 212104 (2015).
28. P. Dongmo, Y. Zhong, P. Attia, C. Bomberger, R. Cheaito, J. F. Ihlefeld, P. E. Hopkins, and J. Zide, "Enhanced room temperature electronic and thermoelectric properties of the dilute bismuthide InGaBiAs Enhanced room temperature electronic and thermoelectric properties of the dilute bismuthide InGaBiAs," J. Appl. Phys. **112**(9), 093710 (2012).
29. D. Kandel and E. Kaxiras, "The Surfactant Effect in Semiconductor Thin-Film Growth," in H. Ehrenreich and F. Spaepen, eds., *Solid State Physics* (Academic Press, 2000), Vol. 54, pp. 219–262.
30. J. Massies, N. Grandjean, and V. H. Etgens, "Surfactant mediated epitaxial growth of InxGa1−xAs on GaAs (001)," Appl. Phys. Lett. **61**(1), 99–101 (1992).
31. N. Grandjean, J. Massies, and V. H. Etgens, "Delayed relaxation by surfactant action in highly strained III-V semiconductor epitaxial layers," Phys. Rev. Lett. **69**(5), 796–799 (1992).
32. Y. Zhong, P. B. Dongmo, J. P. Petropoulos, and J. M. O. Zide, "Effects of molecular beam epitaxy growth conditions on composition and optical properties of InxGa1−xBiyAs1−y," Appl. Phys. Lett. **100**(11), 112110 (2012).
33. G. Feng, K. Oe, and M. Yoshimoto, "Temperature dependence of Bi behavior in MBE growth of InGaAs/InP," J. Cryst. Growth **301-302**, 121–124 (2007).

Optical Materials EXPRESS

34. N. Grandjean, J. Massies, C. Delamarre, L. P. Wang, A. Dubon, and J. Y. Laval, "Improvement of the growth of InxGa1−xAs on GaAs (001) using Te as surfactant," Appl. Phys. Lett. **63**(1), 66–68 (1993).
35. I. García, I. Rey-Stolle, B. Galiana, and C. Algora, "Analysis of tellurium as n-type dopant in GaInP: Doping, diffusion, memory effect and surfactant properties," J. Cryst. Growth **298**, 794–799 (2007).
36. T. Kageyama, T. Miyamoto, M. Ohta, T. Matsuura, Y. Matsui, T. Furuhata, and F. Koyama, "Sb surfactant effect on GaInAs/GaAs highly strained quantum well lasers emitting at 1200 nm range grown by molecular beam epitaxy," J. Appl. Phys. **96**(1), 44–48 (2004).
37. T. Sato, M. Mitsuhara, T. Watanabe, and Y. Kondo, "Surfactant-mediated growth of InGaAs multiple-quantum-well lasers emitting at 2.1μm by metalorganic vapor phase epitaxy," Appl. Phys. Lett. **87**(21), 211903 (2005).
38. S. H. Huang, G. Balakrishnan, A. Khoshakhlagh, A. Jallipalli, L. R. Dawson, and D. L. Huffaker, "Strain relief by periodic misfit arrays for low defect density GaSb on GaAs," Appl. Phys. Lett. **88**(13), 131911 (2006).
39. A. J. Ptak, D. A. Beaton, and A. Mascarenhas, "Growth of BGaAs by molecular-beam epitaxy and the effects of a bismuth surfactant," J. Cryst. Growth **351**(1), 122–125 (2012).
40. S. Tixier, M. Adamcyk, E. C. Young, J. H. Schmid, and T. Tiedje, "Surfactant enhanced growth of GaNAs and InGaNAs using bismuth," J. Cryst. Growth **251**(1-4), 449–454 (2003).
41. A. J. Ptak, R. France, C.-S. Jiang, and R. C. Reedy, "Effects of bismuth on wide-depletion-width GaInNAs solar cells," J. Vac. Sci. Technol., B: Microelectron. Nanometer Struct.–Process., Meas., Phenom. **26**(3), 1053 (2008).
42. E. F. Schubert, G. H. Gilmer, R. F. Kopf, and H. S. Luftman, "Maximum concentration of impurities in semiconductors," Phys. Rev. B **46**(23), 15078–15084 (1992).
43. J. E. Northrup and S. B. Zhang, "Dopant and defect energetics: Si in GaAs," Phys. Rev. B **47**(11), 6791–6794 (1993).
44. E. Tokumitsu, "Correlation between Fermi level stabilization positions and maximum free carrier concentrations in III-V compound semiconductors," Jpn. J. Appl. Phys. **29**(Part 2, No. 5), L698–L701 (1990).
45. S. B. Zhang, "The microscopic origin of the doping limits in semiconductors and wide-gap materials and recent developments in overcoming these limits: a review," J. Phys.: Condens. Matter **14**(34), R881–R903 (2002).
46. S. Muto, S. Takeda, M. Hirata, K. Fujii, and K. Ibe, "Structure of planar aggregates of si in heavily si-doped gaas," Philos. Mag. A **66**(2), 257–268 (1992).
47. C. Domke, P. Ebert, M. Heinrich, and K. Urban, "Microscopic identification of the compensation mechanisms in Si-doped GaAs," Phys. Rev. B **54**(15), 10288–10291 (1996).